JOURNAL OF
ENVIRONMENTAL HYDROLOGY
The Electronic Journal of the International Association for Environmental Hydrology
On the World Wide Web at http://www.hydroweb.com
VOLUME 17 2009

HYDROGEOLOGY, HYDROGEOCHEMISTRY, AND GROUNDWATER MODELING OF THE ZILITAN AREA, NORTHWESTERN LIBYA

Mohamed El Kashouty[1]
A. Abdel-Lattif[2]

[1]Cairo university, Faculty of Science, Geology Department
[2]National Research Institute of Astronomy and Geophysics
Helwan, Cairo, Egypt

The management of the limited arid groundwater resource in the Zilitan area, northwestern Libya, is critical. A combined analysis of hydrogeology and hydrogeochemistry is carried out to develop a comprehensive picture of the groundwater basin. There is concern with TDS increases in the north due to seawater intrusion. Principal component analysis identified distinct hydrogeological processes in the system. Dedolomitization was common in the aquifer. The groundwater samples are found to be unsuitable for drinking purposes but they are suitable for irrigation. The Processing Modflow for Windows model estimates a 5 m drop in potentiometric level in the southwest over 10 years at today's pumping rates. We recommend no increase in pumping rate, otherwise seawater intrusion can contaminate the groundwater system even with a small drop in potentiometric level.

INTRODUCTION

More than 50% of the world's population depends on groundwater for drinking (Fry, 2005). The Zilitan area, northwestern Libya (Figure 1) is facing an increase in water demands associated with rapid population, especially on the coast, because of industrial development and expansion of irrigated areas. The northern plains witness high population densities particularly in the coastal strips, where soils are suitable for a wide range of agricultural production. Therefore more than 80% of the Libyan population, estimated at approximately 5 million, is located in the large population centers in both Gefara and Benghazi plains and the other coastal cities. Population densities may exceed 120 persons/km^2 in the north and less than 1 person/km^2 in the desert areas, in the central and southern regions.

This has led to over exploitation of groundwater and results in shortage and poor water quality. Rapidly increasing urban population growth rates over the last few decades have been responsible for the production of huge quantities of wastewater, which are disposed into the groundwater system without treatment. Carbonate aquifers are particularly vulnerable to nitrate contamination from various anthropogenic activities at the land surface. Elevated nitrate concentration has resulted from the application of fertilizers to cropland (Wells and Krothe, 1989; Katz et al., 2001), septic tank leachate (White, 1988; Pacheco and Cabrera, 1997; and Veni et al., 2001), and disposal of animal wastes (Berryhill, 1989; Molerio and Gutierrez, 1999). Water quality monitoring studies of hydrogeology and hydrogeochemistry are undertaken to clarify the impact of anthropogenic and lithogenic sources. The water resources fall under the two major categories, namely the surface and the groundwater resources. The former is rather limited and contributes less than 3% of the total water use for different activities.

GEOLOGY AND AQUIFER SYSTEM

The Sirt basin rift system (includes the study area) is surrounded to the northeast by the Cyrenaica platform and to the south and west by the Paleozoic basins of Al-Kufra, Murzug, and Ghadamis, respectively. The Sirt basin is a cratonic basin, resulting from the extension of an eroded basement and Paleozoic uplift (Suleiman, 2006). It is composed of broad NW-trending features (Suleiman, 1993). Several authors have discussed the geology of the Zilitan area (Goudarzi, 1970; Magnier, 1963; Hammuda, 1967; Burollet et al., 1960 and 1963; and Mann, 1975). The sedimentary succession (Middle Miocene to Quaternary) crops out as shown in (Figure 1). A transgression sequence of Middle Miocene sediments (Al-Khums Formation) overlies disconformably Lower Cretaceous rocks. The Al-Khums formation reflects carbonatic developments of a succession of marl-calcilutite-calcarenite (Figure 2) (Abdel-Lattif et al., 2004). The outcrop of the Al-Khums formation is concentrated mainly in the western, southwestern, and southeastern part of the study area (Figure 1). The Quaternary deposits are divided into Pleistocene (Gargaresh formation) and Holocene deposits (wadi, eolian, and fluvioeolian deposits). The aquifer is the Al-Khums formation under semi confined to confined conditions. The continuous thickness of the clay increases in the northeastern part (Figure 2). The formation is fractured, which is attributed to tectonic activity during the Hun graben (Salem et al., 2000). Groundwater recharge (by rainfall) occurs where the aquifer crops out in the western, southwestern, and southeastern part. The groundwater flow is generally away from the recharge area (west-central) towards the north (main flow) and southwest (local flow) (Figure 3a). The study area is characterized by a temperature range of 6 to 46 ^{o}C in the winter and summer seasons. Moisture content ranges from 63 to 82 %, annual evaporation in eastern Hamada basin (included the study

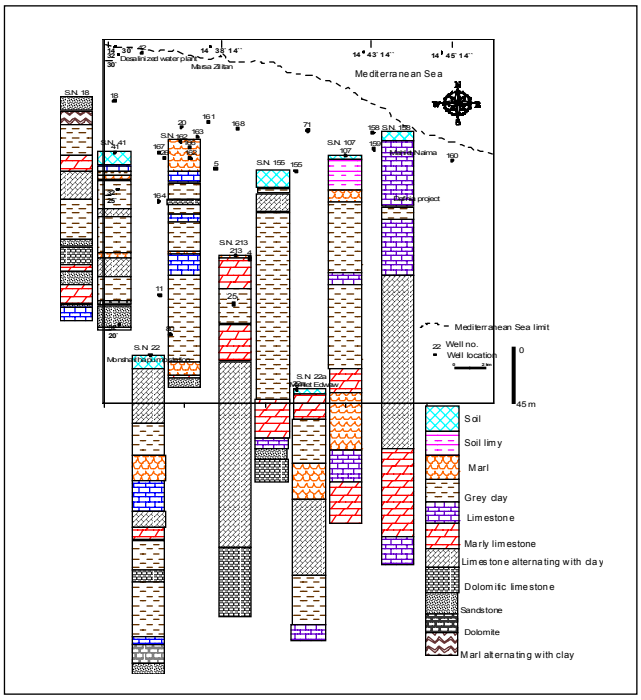

Figure 1. Well location map and lithological column.

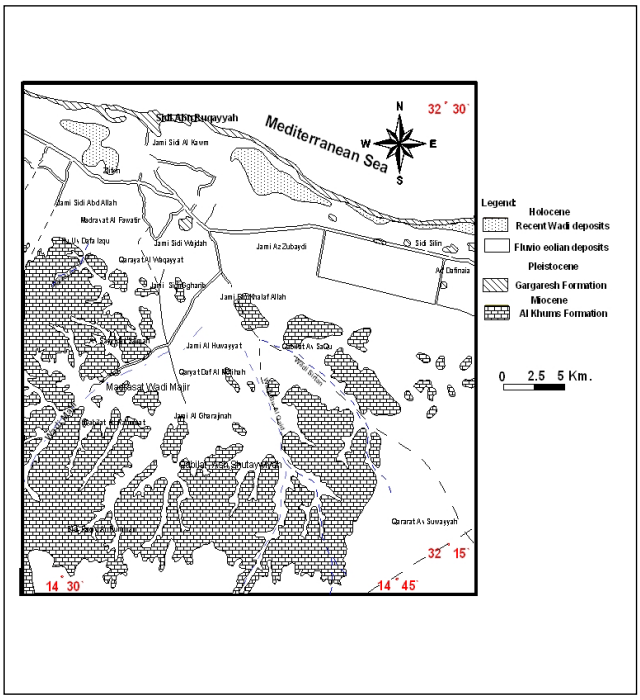

Figure 2. Geologic map of the Zilitan area, northwestern Libya (after El-Hinnawy and Chesthitey (1975)).

area) is more than 1500 mm (Burdon and Gonfiantini, 1991). The north coastal strip is situated under a semi-Mediterranean climate and receives winter rainfalls ranging from 200 to 400 mm/yr (Salem, 2004).

The aquifer is renewable (Figure 4) and has high precipitation rates. The northern aquifers contribute more than 2400 Mm^3/yr against an annual recharge of less than 650 Mm^3/yr.

This imbalance introduces continuous lowering of groundwater levels accompanied by deterioration in water quality due to seawater intrusion and invasion of saline water from adjacent

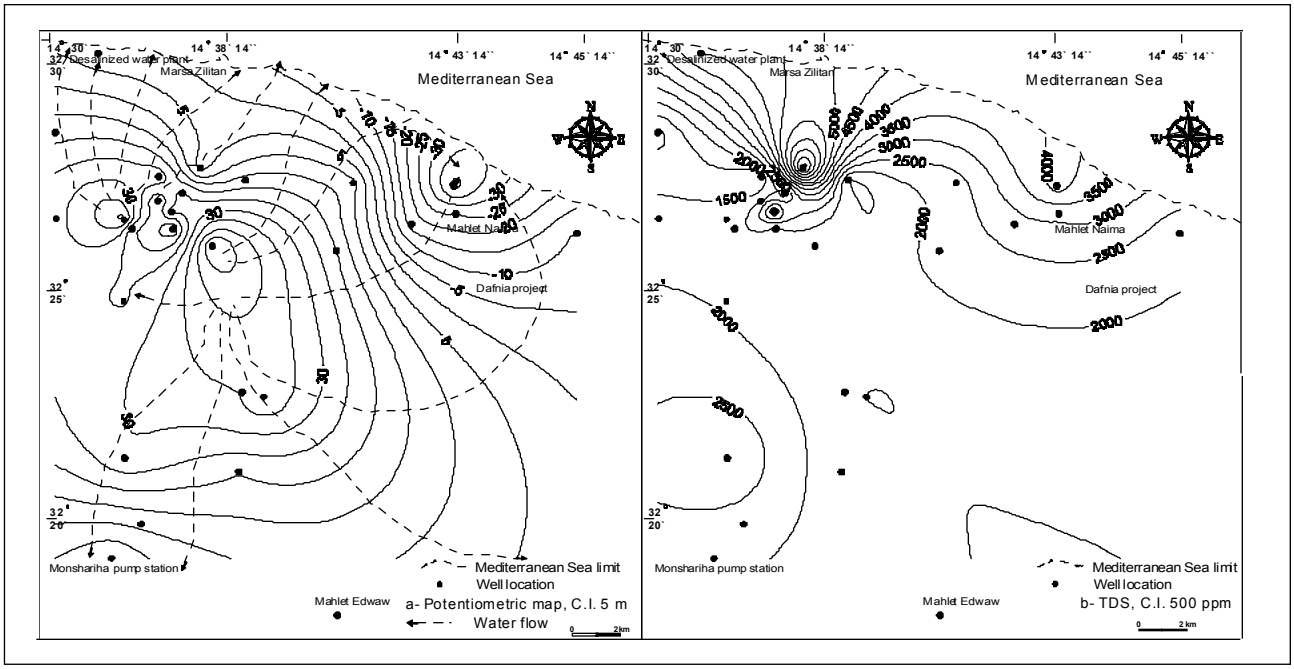

Figure 3. Potentiometric map (a) and total dissolved solids (b) of the aquifer, northwestern Libya.

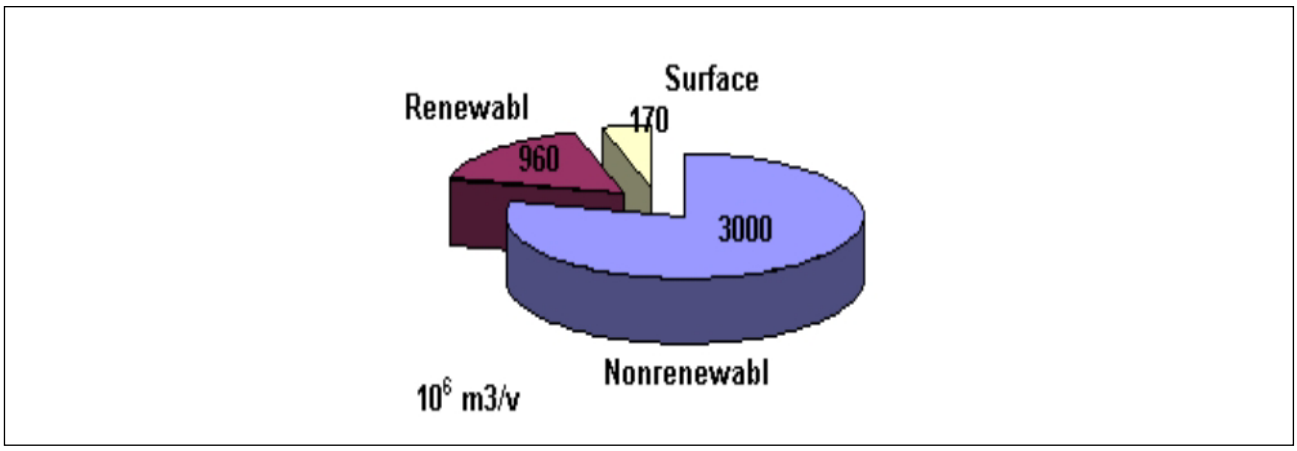

Figure 4. Potential water resources (after Salem, 2004).

aquifers. Recently, several well fields were developed to supply the Great Man Made River Project (GMMRP). When completed, the GMMRP will supply more than 6 Mm^3/day to the agricultural fields and population centers in the north of Libya. According to the hydrogeological studies, GMMRP water will minimize the water balance deficits in the effected zones (Salem, 2004).

MATERIALS AND METHODS

Data of nine pumping wells, having depths ranging from 142 to 350 m, obtained from the Libyan Public Committee for Housing and Infrastructures are available for lithology, step, constant, and recovery tests. The chemical analysis of 26 groundwater samples was obtained from the same authority. The investigation of these data has been carried out by the authors, using hydrogeochemical, hydrogeological, PMWIN, and AquaChem programs. The transmissivity has been calculated by software using constant and recovery tests.

RESULTS AND DISCUSSION

1. Hydrogeological characteristics.

Drawdown in wells is composed mainly of two components, the formation loss and the well loss. A more sophisticated method for analysis proposed by Jacob (1946) and Bierschenk (1964) is based on the relationship: $S_w = BQ + CQ^2$, where S_w is the drawdown in the pumping well (in m), Q is the discharge rate (in m^3/d), BQ is the formation loss. The amount of drawdown resulting from the aquifer permeability (in m) and the CQ^2 is the well loss, i.e. the amount of drawdown resulting from the hydraulic resistance of the well screen/well face (in m). The formation loss depends on aquifer hydrogeological characters, while the well loss is influenced by design and construction of the well, choice of filter pack materials, length of screen and proportion of open area, well penetration, efficiency of the well development, and discharge rate. Doubling the latter, can increase the well loss four fold (Jacob, 1946): $S_w/Q = B + CQ$. The transmissivity and formation and well losses are estimated by the authors using step, constant, and recovery tests (Figure 5).

a) Drawdown and transmissivity.

The drawdown increases in the northern and northeastern part of the study area (Figure 6a) due to the increase in thickness of continuous clay, lack in interconnection of joint and fracture systems, and the increase in pumping rate. On the other hand, in the southwestern and eastern part, low drawdown (Figure 6a), is attributed to dissolution of the exposed limestone aquifer via rainfall which enhances the joint and fracture systems for interconnection. The transmissivity increases

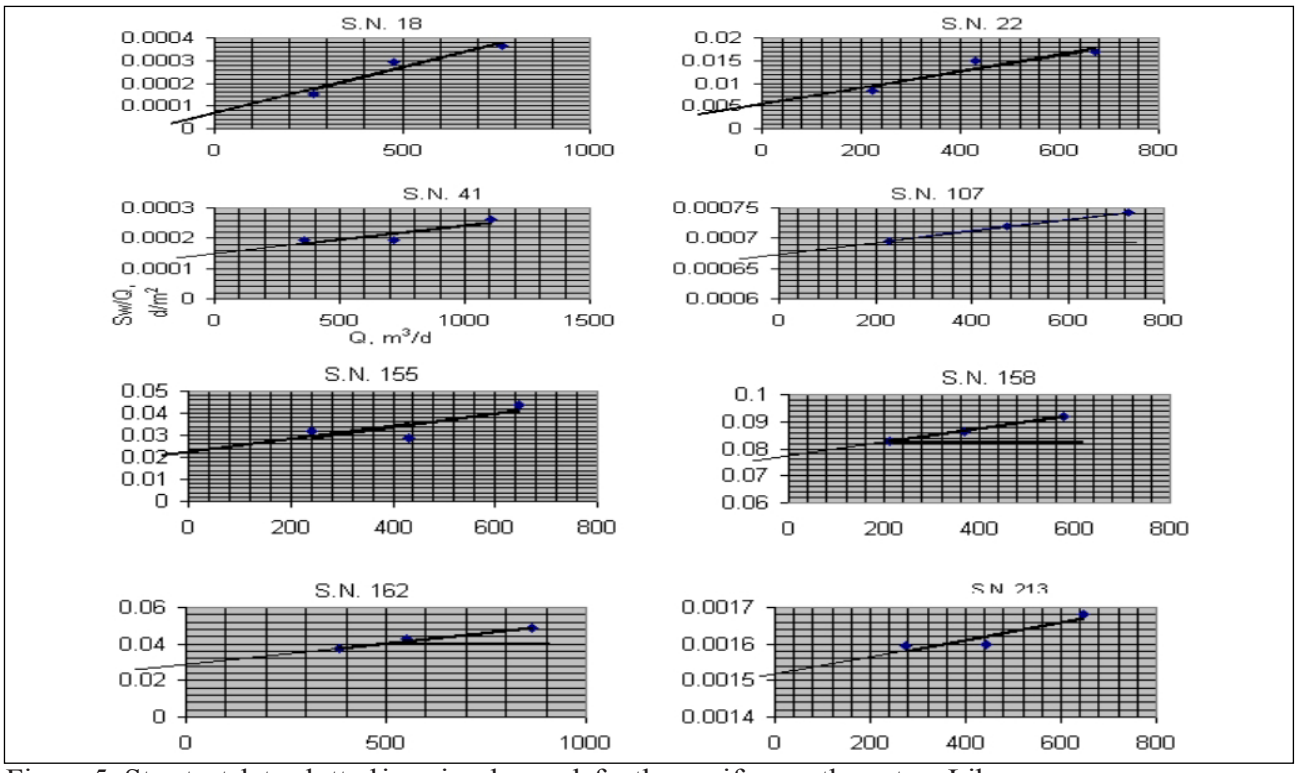

Figure 5. Step test data plotted in a simple graph for the aquifer, northwestern Libya.

in the western and eastern part (Figure 6b), because of more dissolution of the exposed limestone enhancing the hydraulic conductivity in the limestone aquifer system. Water in the carbonate rock aquifer is primarily present in fracture, joints, bedding planes, and solution channels within the rock. These openings are due, in part, to the effects of weathering during the period of geologic history when the aquifer was exposed at the land surface (western, southwestern, and southeastern parts, see Figure 1). The transmissivity locally increased in the northeastern zone due to vertical inflow from the overlying sediments into the aquifer system.

b) Formation and well losses.

Formation and well losses increase in the northern part (Figure 6 c and d), due to high thickness of the clay and low exposed limestone. The western, southwestern, and southeastern parts are characterized by more dissolution of the exposed limestone that reduces the formation and well losses. The northeastern zone is characterized by different trends, formation and well losses increases in the northeastern part (Figure 6c), while they decrease locally in the center of the northeastern zone (Figure 6d). It may be inflow from the overlying sediments into the aquifer system that increases the transmissivity and decreases the formation and well losses. Also the increase in well loss in the northern part is attributed to poor well design.

c) Recovery test.

Samples 22 and 158 are recovered after the longest periods (Figure 7), and confirm the lack of interconnection in joint and fracture systems. While samples 162 and 155 recovered after short periods (Figure 7). A vertical hydraulic gradient eventually may develop initiating vertical drainage from the overlying beds (limestone layer alternating with clay) which contains substantial storage.

A low rate of drawdown (right wells in Figure 7) indicates good hydraulic conductivity and storage capacity. These wells show rapid recovery (Figure 7) except well 231, and this may be attributed to good storage and lack of interconnection of joint and fracture systems.

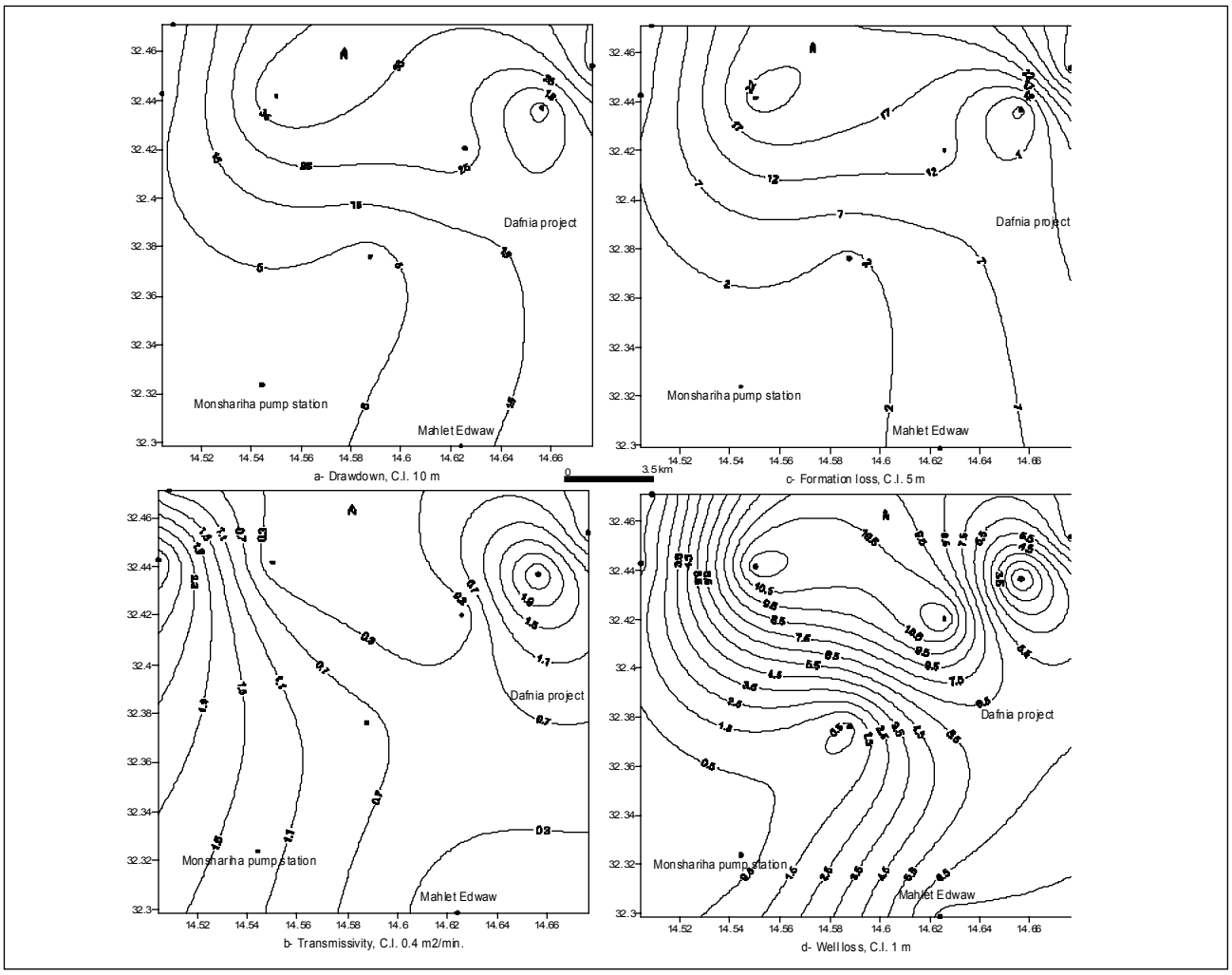

Figure 6. Hydrogeological characteristics of the aquifer, northwestern Libya.

d) Constant and step tests

Figure 7 illustrates the constant discharge at the same pumping rate of step discharge imposed in 3-4/120-min steps with incremental discharge. Despite the same discharge in stepped pumping, the equilibrium drawdown is lower than those in the case of constant discharge. A comparison of the specific drawdown (s/Q) for constant discharge and s'/Q' for step discharge for the wells examined is presented in Table 1, together with a summary of well design data. In all cases, an improvement in the specific drawdown (s/Q) resulted from phased pumping. The percentage reduction varied from one well to another, but this was not unexpected and depends upon borehole design/completion, and differences in the hydrogeology, thickness, and degree of fracturing and jointing. The highest drawdown plot is in the case of constant discharge, where 75 % of the equilibrium drawdown occurred in the 1st 360 minutes of pumping. This drawdown is largely the result of withdrawal from well storage arising probably because the initial flow from the aquifer was insufficient (due to low storage in the fracture and joint systems) to meet the imposed pumping. It is caused by low exposed limestone in that area and a low amount of dissolution that reduces the joint and fracture interconnection in the limestone system.

2. Hydrogeochemical characteristics

Geochemical data can evaluate the interrelationship among groundwater chemistry, aquifer mineralogy, and groundwater flow. Figure 3b shows the distribution of the TDS. It increases in the

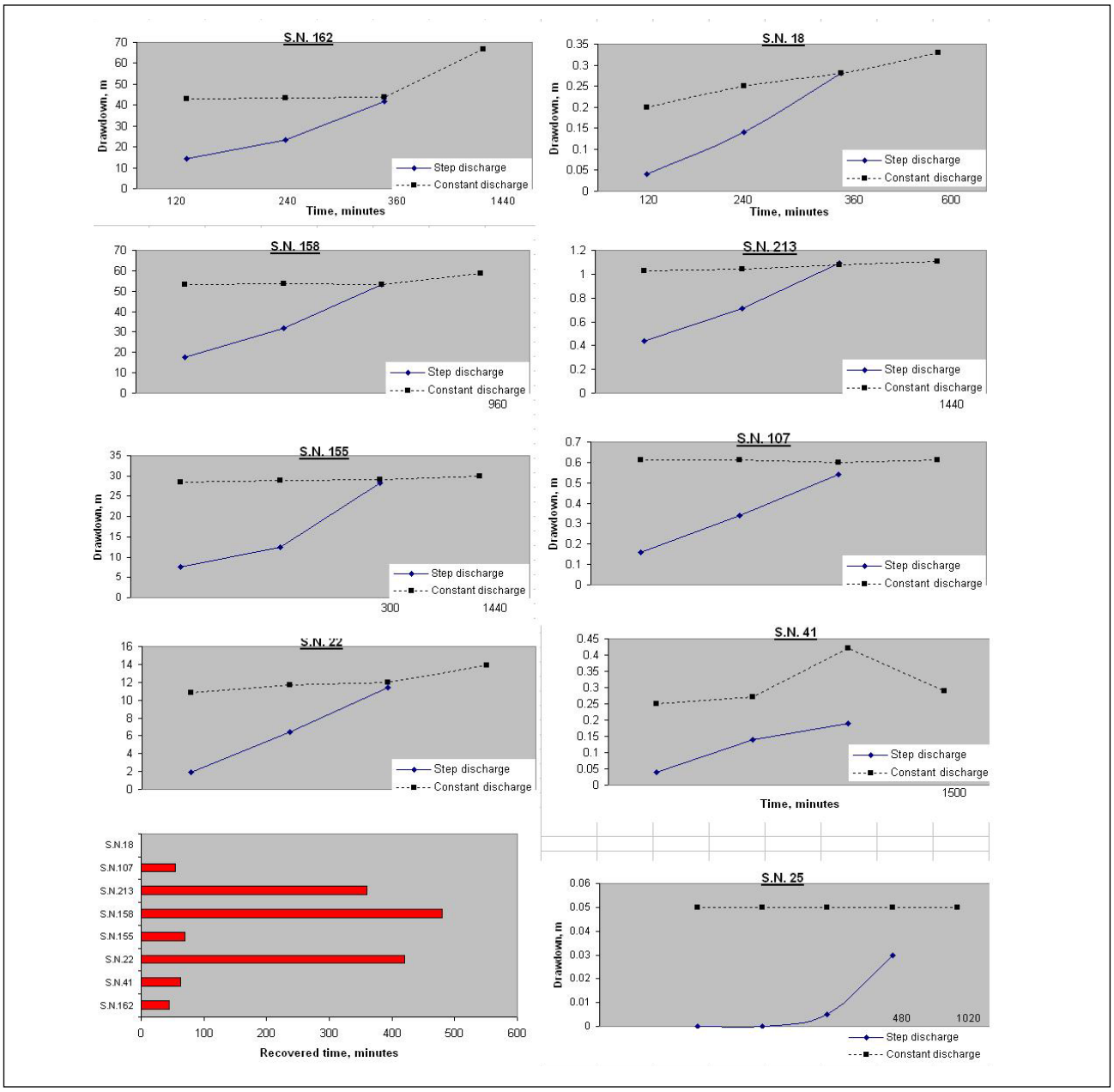

Figure 7. A comparison of drawdown plots for step and constant discharge and recovery data.

northern part. The highest concentration is in the northwestern part, while a high concentration is in the northeastern part (see Figure 3b). TDS increased along the flow path (see Figure 3a) from the surface to the saturated zone and through the aquifer system because of dissolution of minerals (Freeze and Cherry, 1979). Additional processes such as evaporation, evapotranspiration, or seawater intrusion, can increase concentration of solutes. Dissolved solids and sulfate concentrations have been used as indicators of chemical evolution of groundwater in various regional scale carbonate aquifers, such as the Floridian aquifer in Florida, the Edwards aquifer in Texas, and the Madison aquifer in parts of Montana, south Dakota, and Wyoming (Plummer et al., 1976; and Busby et al., 1991). The high continuous thickness of the clay layer (Figure 2), in the northeastern part, reduces the seawater intrusion rate, rather than in the northwestern part. The hotspot (TDS) in the northeastern part coincides with the highest NO_3 content (see Figure 8e), indicating agricultural seepage which is responsible partially for the groundwater degradation. An exciting feature of this aquifer system is the well defined patterns of variability in the major ions.

Table 1. Percentage improvement in s/Q and summary data.

	Constant discharge test data						
Borehole No.	Discharge rate (Q, m^3/h)	Equilibrium drawdown (s, m)	Pumping Duration, min	Specific drawdown (s/Q)			
107	30.3	0.61	1440	0.02			
213	27	1.11	1440	0.041			
158	24	58.6	960	2.44			
155	27	29.97	1440	1.11			
22	28	13.85	1440	0.49			
41	46	0.29	1500	0.006			
25	25.2	0.05	1020	0.002			
18	32	0.33	600	0.01			
162	36	66.63	1440	1.85			
	Step discharge test data						
Discharge rate Q'	Equilibrium drawdown (s', m)	Pumping duration, min	Specific drawdown (s'/Q')	% changed in s/Q	Well depth, m	Cased thickness m	Screened thickness m
30.3	0.54	360	0.018	10	262	226	30
27	1.09	360	0.04	2.4	291	224	61
24	53.03	360	2.21	9.4	350	250	94
27	28.26	300	1.05	5.4	250	200	44
28	11.41	360	0.41	16.3	202	172	24
46	0.29	360	0.006	0	142	94	45
25.2	0.03	510	0.001	50	256	190	60
32	0.28	360	0.009	10	180	130	44
36	41.94	360	1.17	37	200	158	39

The TDS (Figure 3b) and Na (Figure 8a) contents change markedly along the major flow system (Figure 3a). TDS increased significantly with groundwater flow in the northern part. Carbonate dissolution and ion exchange occurred leading to the variation of water types, including the seawater intrusion impact. It can be concluded that the hydrogeology (groundwater flow, see Figure 3a) coincides with the hydrogeochemistry (TDS map, see Figure 3b). Mg concentration increased in the northwestern and southwestern part (Figure 8b), attributed to seawater intrusion for the former and carbonate-gypsum sediment dissolution for the latter. SO_4 content increased in the southwestern part (Figure 8c), resulting from the dissolution of the carbonate and gypsum deposits. Mg and SO_4 concentrations increased in the southwestern part enhanced by the groundwater flow in that part. HCO_3 content increased in the northern and northwestern part (Figure 8d). Sulfate reduction may explain the increase in HCO_3 and decline in SO_4 concentrations in the northwestern part. The most reasonable explanation of the patterns (Figure 8c and d) is a geologic one. The increase in HCO_3 concentration in the northwestern part also may result from reduction of organic matter.

NO_3 content increased in the northeastern part (Figure 8e), because of seepage of agricultural, sanitary, and septic tank wastewaters. K concentration increased in the northeastern and southwestern part (Figure 8f), attributed to anthropogenic and lithogenic sources, respectively. The chemical evolution in the main recharge area (see Figure 3a) can be explained by direct infiltration of precipitation with subsequent uptake of CO_2, resulting in the dissolution of limestone and marlite.

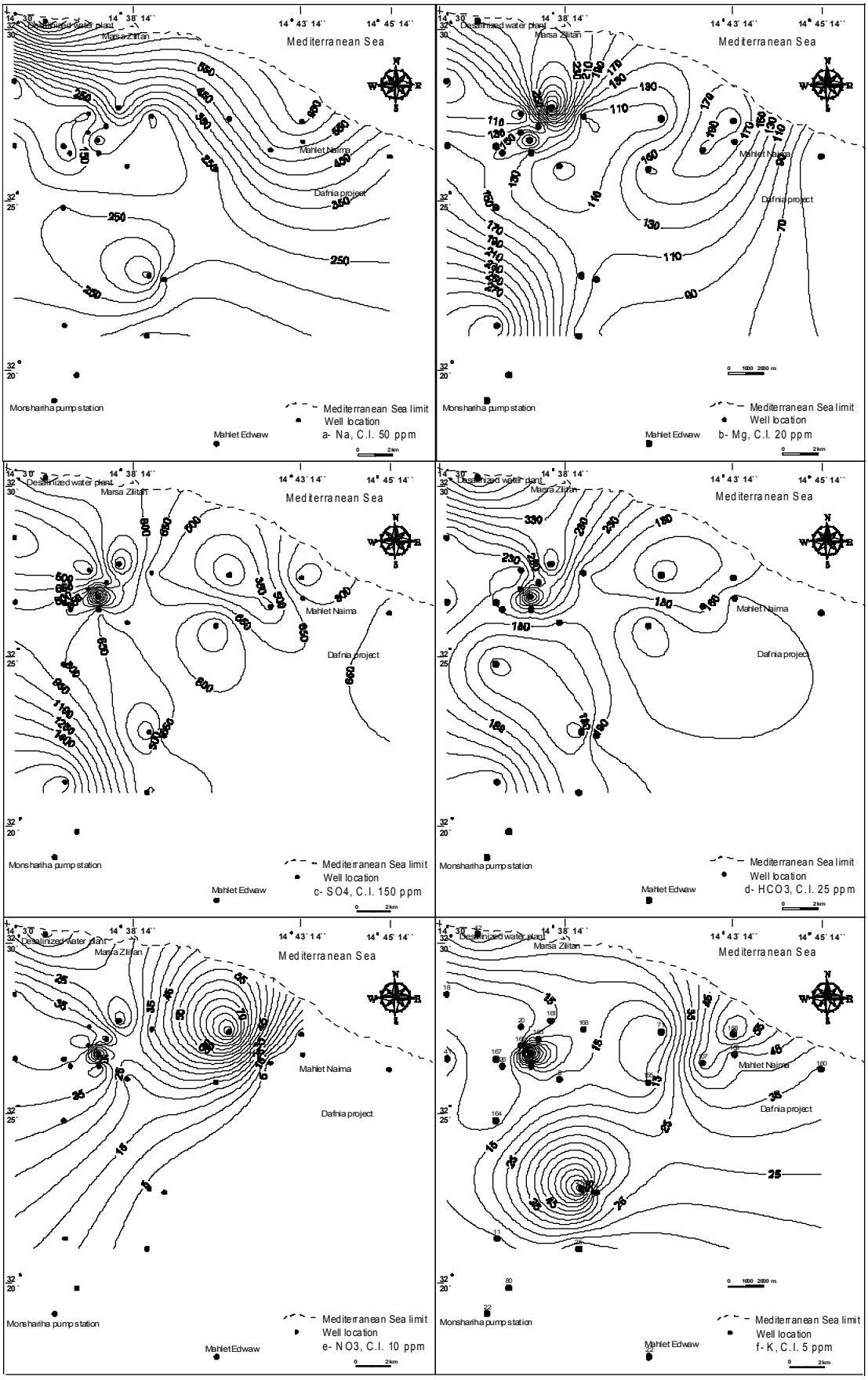

Figure 8. Major ions distribution in the aquifer, northwestern Libya.

The hydrolysis and dissolution reactions of limestone and dolomite to form dissolved bicarbonate, calcium, and magnesium, are described by Appelo and Postma (2005).

$CaCO_3 + H_2O \rightarrow Ca2^+ + 2HCO_3^- + OH^-$

$CO_2 + H_2O \rightarrow HCO_3- + H+$

$CaMg\ (CO_3)_2 + 2H_2o \rightarrow Ca^{2+} + Mg^{2+} + 2HCO_3^- + 2OH^-$

$2CO_2 + 2H_2O \rightarrow 2HCO3^- + 2H^+$

The molar Mg/Ca ratios in groundwater are lower than 0.8, except 3 samples in the northern part. It suggests that dissolution of limestone ($CaCO_3$) is faster than magnesium, and no calcite precipitation is available, confirmed by the saturation index estimation.

3. Multivariate statistical analyses

The Pearson coefficients (PC) and the principle component analysis (PCA) (Shine et al., 1995; Ruiz, 2001; Liu et al., 2003; and Zhou et al,. 2004) have been conducted using SPSS for Windows Ver. 12.0 in order to study the interrelationship among the chemical elements. The varimax method is chosen as the rotation method for PCA. Factor analysis of different sets (depending on selected variable and cases) have identified 4 factors with Eigen values >1, which formally can be assessed as statistically significant factors. Factor 1 is positively loaded with TDS, HCO_3, SO_4, Cl, Na, Mg, and Ca, and negatively with NO_3 (Figure 9). It reflects the lithological impact of limestone, gypsum, and clay sediments and seawater intrusion for the first and denitrification process for the second. These elements enhance the denitrification process. Factor 1 can be interpreted as a factor of influx of more saline sulfate groundwater from the aquifer and seawater intrusion. Factor 2 includes positively K and pH, and may result from partially lithogenic source. Factor 3 contains positive SO_4, Ca, and water depth, clarifying the dissolution of carbonate and gypsum sediments included in the aquifer system with depth. Factor 4 is positively loaded with pumping rate, and delineates that the discharge rate doesn't affect groundwater hydrogeochemical processes. TDS is strongly correlated with Cl, Mg, Ca, and moderately with HCO_3 and SO_4. This reflects the lithogenic and evaporation influence for the 1st case and rock-water interaction for the 2nd. The groundwater salinity is partially enhanced by dissolution of carbonate sediments, anthropogenic impact, and seawater intrusion. The NO_3 is moderately correlated with K and may attributed to fertilizers. SO_4 is strongly correlated with Ca and Mg, indicating dissolution of the aquifer. Cl is strongly correlated with Na and Mg; showing that Mg may be contributed to by evaporation processes.

4. Saturation indices approach

The state of equilibrium between groundwater and calcite, dolomite, and other minerals in the aquifer system can be evaluated by the computation of saturation indices (SI), expressed as; $SI_{mineral}$ = log (IAP, ion activity product/ Kt, thermodynamic equilibrium constant) (Plummer et al., 1976). Nearly all the recharge area has TDS values that are low (Figure 10a) and the water is under saturated to equilibrium with calcite and dolomite. TDS is higher in the north due to anthropogenic sources and dissolution. The majority of water samples appear to be oversaturated with both minerals, which suggests that both minerals are present in the aquifer system. The saturation indices for calcite and dolomite generally correlate with dissolved solid concentrations (Figure 10a). Figure 10b showing evolving composition in the aquifer illustrates how the composition simply proceeds toward equilibrium with respect to those minerals available for

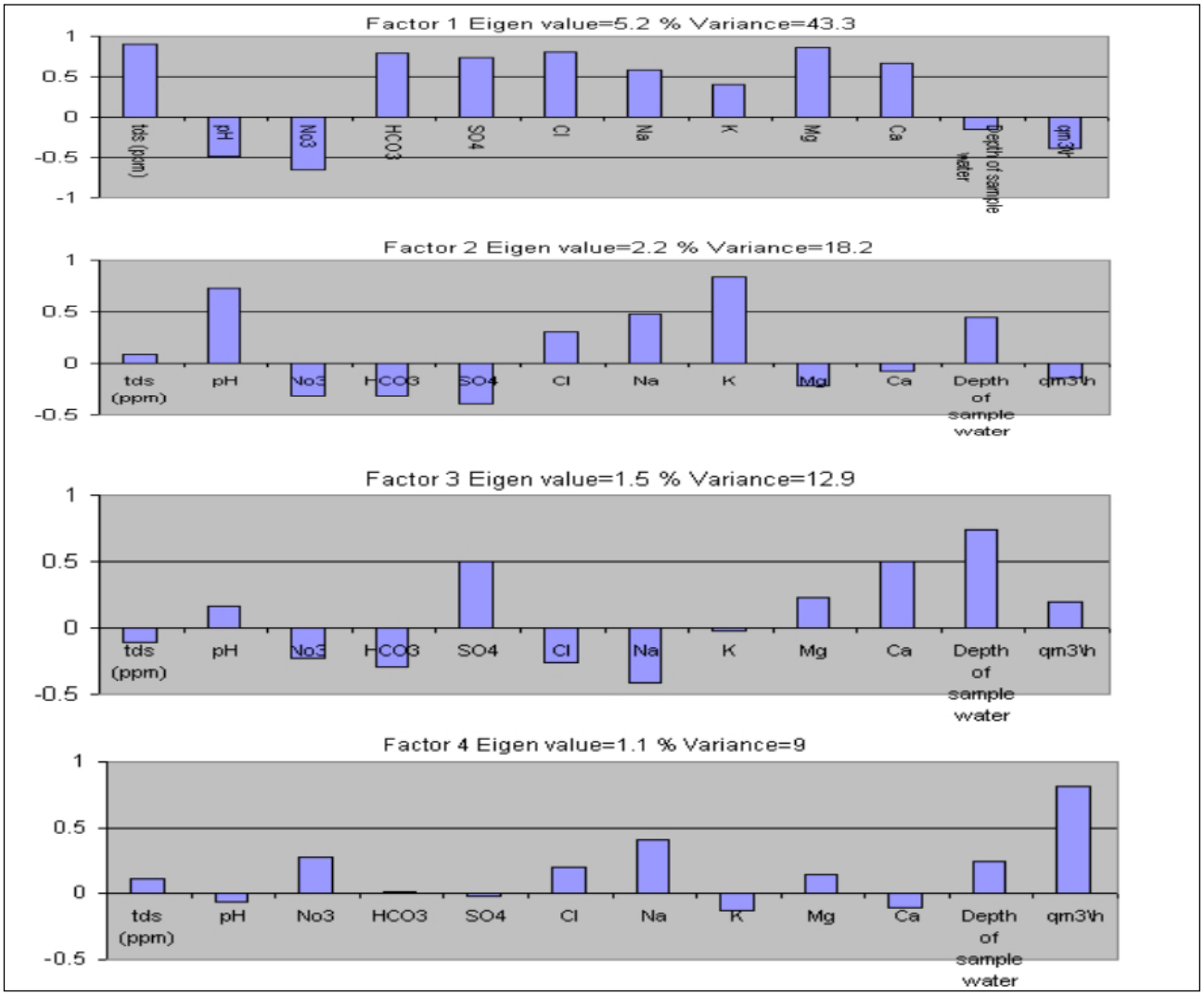

Figure 9. Factor analysis of the major ions in the aquifer system.

dissolution (e.g. calcite and dolomite). The samples reflect the relative length of flow systems. The total CO_2 of the groundwater vs. SI of calcite is depicted in Figure 10c to show the gradual change in CO_2 concentration from atmosphere to the present state. The saturation indices of selected minerals are illustrated in Figure 10d and e.

5. Dolomitization and dedolomitization processes

The reaction of calcite and dolomite with water and CO_2 can be written as follows:

$CaCO_3$ (calcite) + H_2O + $CO_2 \rightarrow Ca^{2+} + 2HCO_3$

$CaMg(CO_3)_2$ (dolomite) +$2H_2O$ + $2CO_2 \rightarrow Ca^{2+} + Mg^{2+} + 4HCO_3$

Typically CO_2 is derived from the oxidation of organic matter and root respiration in the soil zone and is dissolved by recharge water. If dolomite dissolves according to the last equation, the molar proportions of [Ca+Mg] to [HCO_3] should be linear, with a slope of 0.5 (Sandra and George, 2000). No correlation exists between both parameters (Figure 11a), which reflects that the dolomite dissolution process was out the aquifer system. They are highly enriched in calcium and magnesium relative to bicarbonate ([Ca+Mg/HCO_3] > 0.5). The predominant water types are the Ca, Mg-SO_4 and Ca, Mg-Cl, which are characterized by high concentrations of dissolved solids, calcium, magnesium, and sulfate. The predominance of sulfate over HCO_3 and the lack of

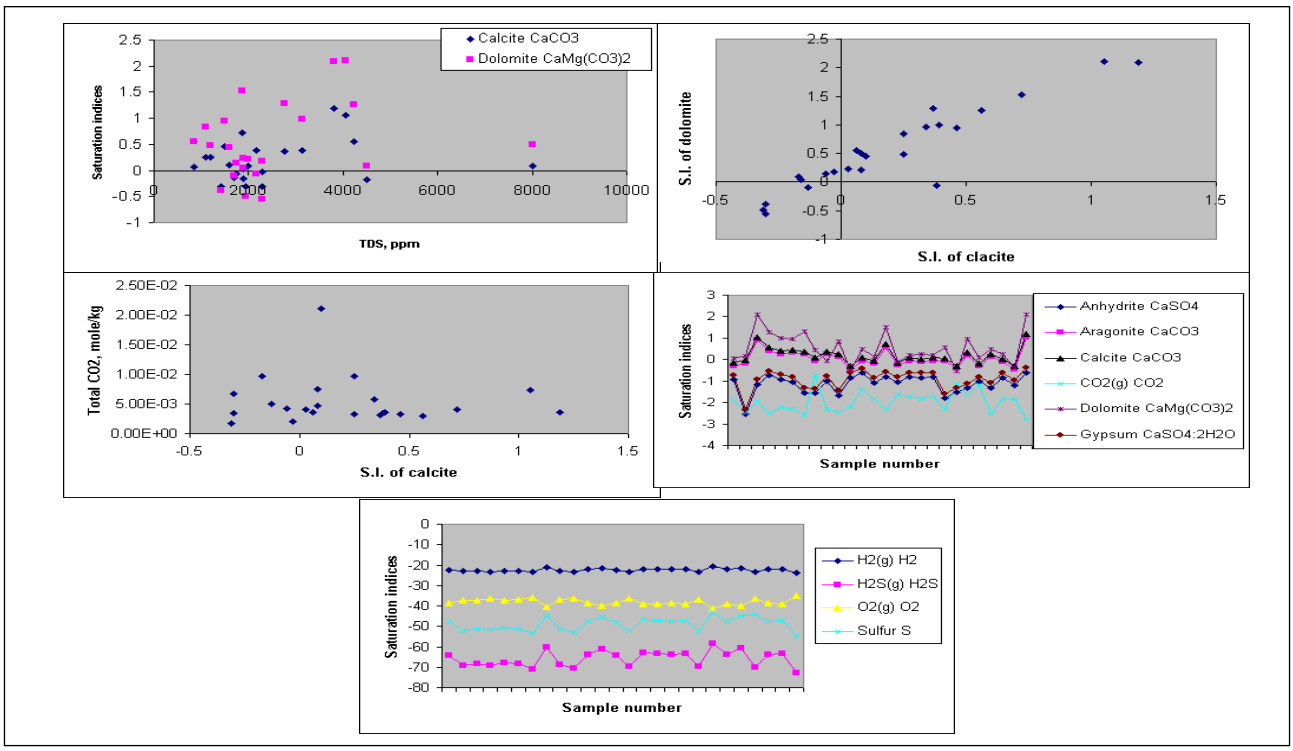

Figure 10. Saturation indices application in the quifer system.

agreement of the previous water types with the simple dolomite dissolution model (Figure 11a) indicates that other processes are controlling the chemistry of these water types.

Two reactions can produce these water types 1) the dedolomitization process, which involves dissolution reactions with carbonate minerals and gypsum, and 2) sulfuric acid neutralization, which involves dissolution of carbonate minerals with sulfuric acid generated by the oxidation of pyrite. On a plot of [Ca+Mg] as a function of [SO_4+0.5HCO_3], the dedolomitization reaction yields a straight line with a slope of 1. There is agreement between the samples trend and the dedolomitization models (Figure 11b), which indicates that this process is more common in the environment. The results of investigations of the other regional carbonate aquifers show that dedolomitization may be a controlling process (Back et al., 1983; and Busby et al., 1991). Groundwater that moves through the aquifer initially dissolves calcite, dolomite, and gypsum (or anhydrite). Once calcite and dolomite reach saturation, gypsum is still undersaturated and continues to dissolve, adding calcium and sulfate to the water. Consequently, calcite becomes oversaturated and, as it precipitates the bicarbonate concentration decreases. The decrease in

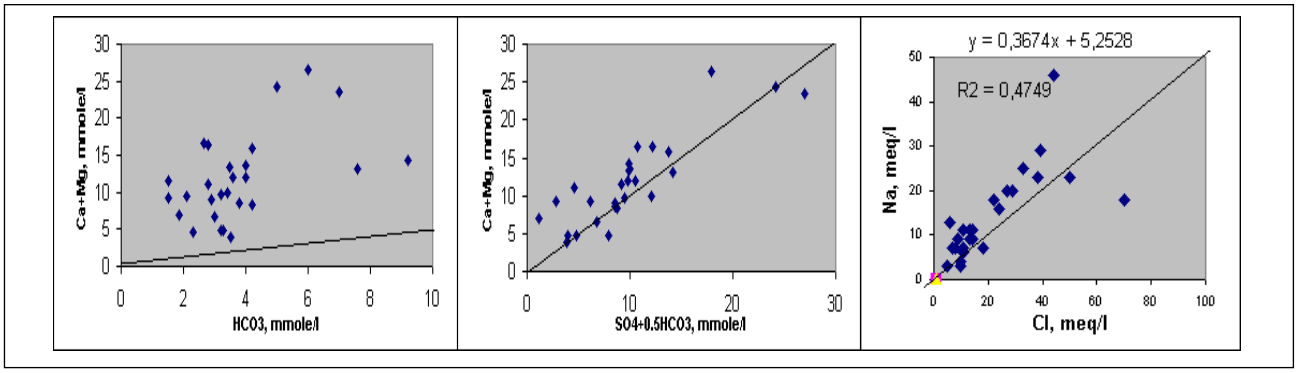

Figure 11. Dolomitization (a), and dedolomitization (b), and Na-Cl relationship models model of the aquifer.

bicarbonate concentration causes the water to be under saturated with respect to dolomite and promotes dissolution of dolomite. In the scatter diagram of Na vs. Cl (Figure 11c), all water samples are plotted close to the seawater dilution line. This illustrates the high evaporation in the environment, since the samples are plotted in the high concentration side closer to seawater dilution (=evaporation) line.

6. Groundwater use

The groundwater is unsuitable for drinking purposes except samples 18, 20, and 23, based on drinking water quality regulations (AquaChem output, Table 2). The irrigation use of the groundwater can be classified into 4 groups (Figure 12). The C_3-S_1 class shows medium to high saline water with low SAR. It is satisfactory for plants having a moderate salt tolerance on soils of moderate permeability with leaching. C4-S1, water of very high salinity and low SAR; water of very high salinity and medium SAR (C4-S2); and C4-S3, water of very high salinity and SAR. The first three classes can be used for all soils particularly those of good permeability and moderate drainage (El Shamy and Abdel Kader, 1999). The C4-S3 class must be used under high drainage condition.

Results of the chemical analysis are presented on a trilinear diagram (Figure 13a), it shows that water type changes as dissolved concentrations change. It indicates chemical homogeneity with a sulfated sodic facies and an enrichment of chloride. The dissolved solids concentrations increase as the percentage of sulfate in water increases. Two chemical types of groundwater are apparent from the Piper (Piper, 1944) diagram (Figure 13a), Na-SO_4-Cl and Ca-Na-Mg-HCO_3-Cl-SO_4. It is confirmed by the Durov (Durov, 1948) and Schoeller (Schoeller, 1963) diagrams (Figure 13 b and c).

7. Groundwater Management Model (Processing Modflow Window application, PMWIN)

The amount of groundwater is sufficient for development, and therefore precludes the need for increase in the discharge rate in the future. Seawater intrusion can contaminate the groundwater system if there is no management of the pumping rate. The model is able to clarify a hydrologic system or to predict the outcome of a future change to the hydrogeological system by the current discharge. The modeled area (Figure 14 a) has a nearly square shape with dimensions of 21000 by 22000 m; it is divided by a grid of 55 by 52 rows and columns; the cell size is 380 x 380 m. The northern part (Mediterranean Sea) is a constant-head boundary. The southwestern, northeastern, and central parts are constant head boundaries; the simulated aquifer is a part of a larger aquifer. The conceptualized model is composed simply of one confined to semi-confined aquifer of non-regular thickness, which is derived from the topographic and lithological data. The hydraulic conductivity is input over the domain area from the 9 pumping wells. A layer type is partially convertible between confined and unconfined. Transmissivity of each cell varies with the saturated thickness of the aquifer. Top and bottom of the aquifer are input to the model.

Table 2. Drinking water quality regulations by AquaChem (US salinity laboratory Staff,1954).

Drinking Element	Quality Recommended	Regulations Maximum
Cond	<400	<1250
TDS	100-500	<1500
Na	<20	
K	10--12	
Mg	<30	<50
Ca	<100	
Cl	<20	<200
NO3	<25	<50

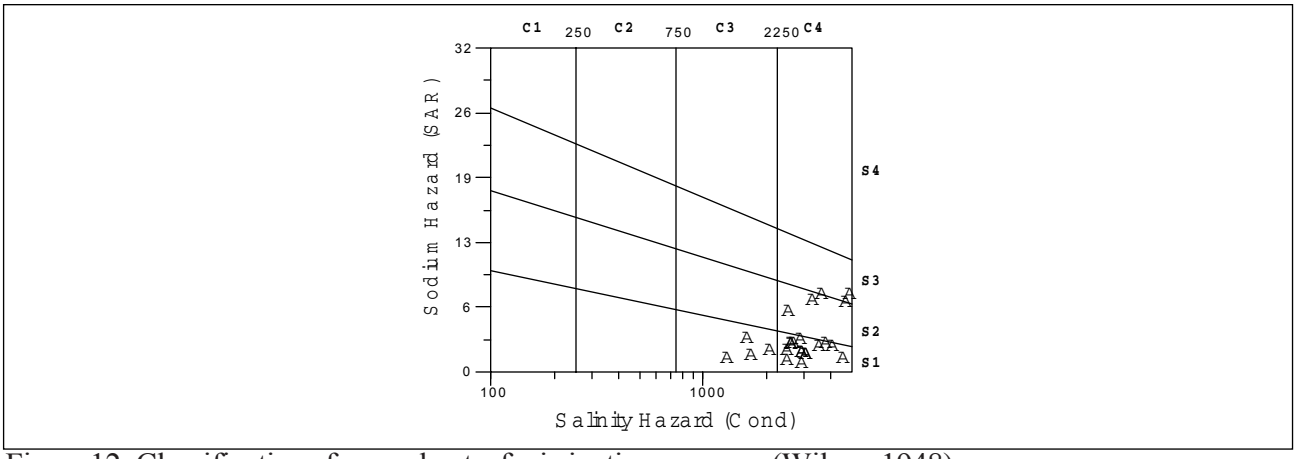

Figure 12. Classification of groundwater for irrigation purposes (Wilcox,1948).

a- Final model design and calibration

The model discretization and parameters are provided in Table 3. The model parameters and/or excitations can be adjusted until model-generated numbers fit the observed values as closely as possible. It searches an optimal parameter set for which the sum of squared deviations between model-generated observations and experimental observations is reduced to a minimum (Figure 14 b).

b- Water budget

For checking the simulation results, MODFLOW calculates a volumetric water budget for the entire model at the end of each time step (Table 4). A water budget provides an indication of the overall acceptability of the numerical solution (Chiang and Kinzelback, 1996). In numerical solution techniques, the system of equations solved by a model actually consists of a flow continuity statement for each model cell. Continuity should also exist for the total inflows and outflows of the entire model or a sub region. This means that the differences between the in- and out- flows should be equal to the total change in storage. The water budget is calculated for layer 1, zone 1 (Table 4). The estimated percent discrepancies of the in- and out- flows for the model is small and acceptable, so the model is correctly solved.

c- Prediction of future conditions

The predicted water level after 10 years at the same current discharge rate is illustrated in (Figure 15 b). It shows a drop in water level of about 5 m in the southwestern part, that can be

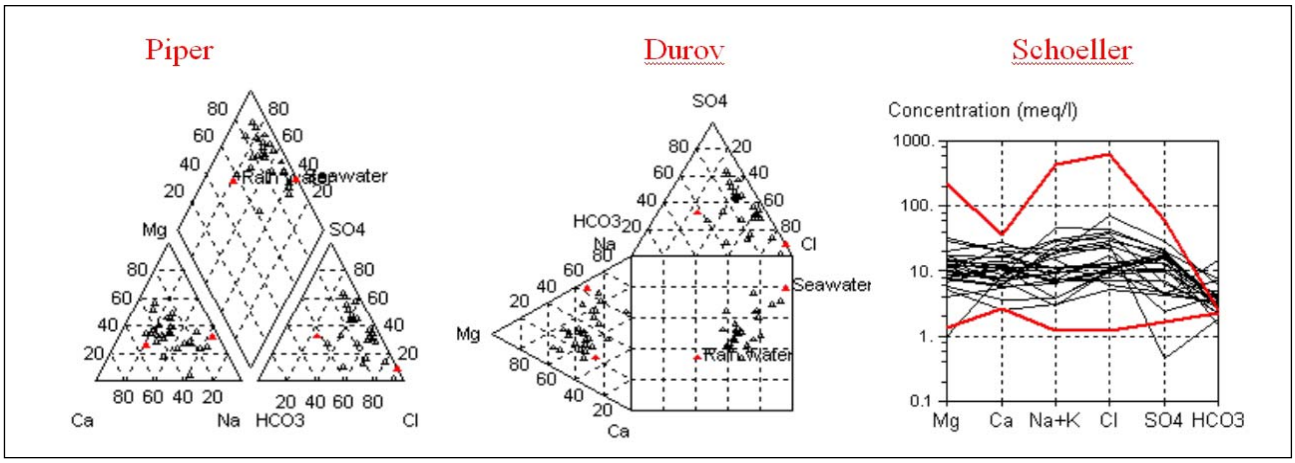

Figure 13. Hydrogeochemical facies in the aquifer.

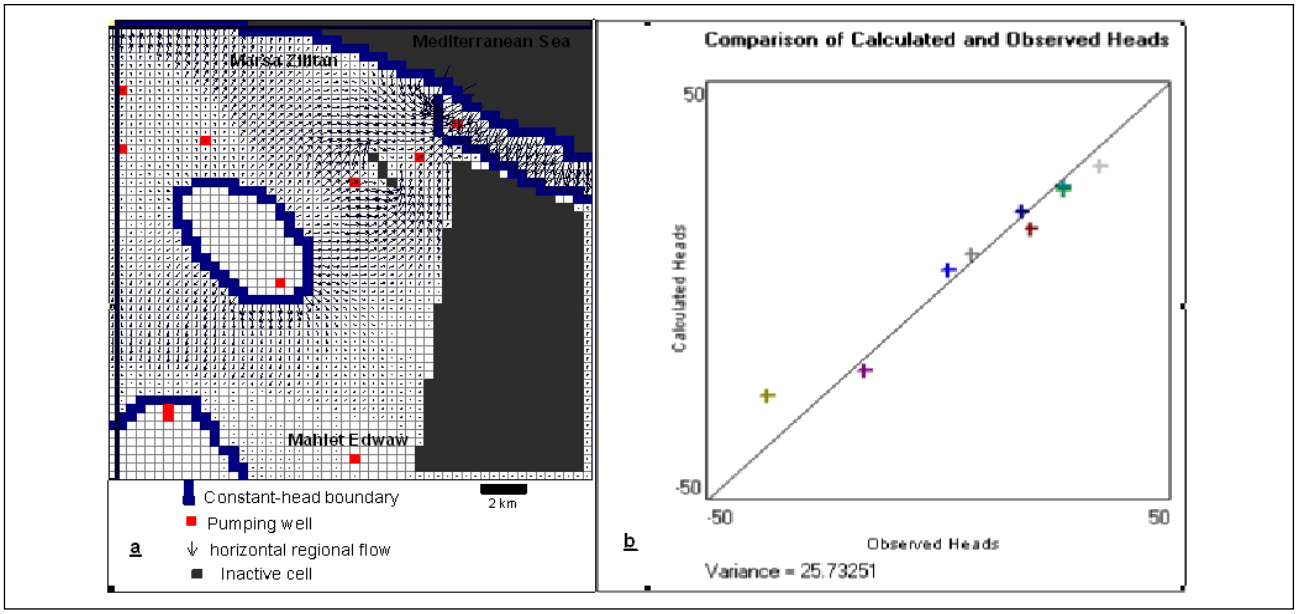

Figure 14. The modeled area of northwestern Libya (Zilitan) (a) and calibrated potentiometric heads (b).

attributed to much recharge from the rainfall into the surface exposure of limestone aquifer. In the northeastern part there is a small drop in potentiometric level, because of seawater intrusion accompanied any drop in hydraulic heads by pumping. The seawater intrusion problem restricts the increase in discharge rate to preclude groundwater pollution. The model predicts the future conditions with the current pumping rate (Figure 15 b). For example, the higher increase in pumping rate in the Nile Delta, Egypt, enhances seawater intrusion as far as Tanta to contaminate the groundwater system. Effects on water quality may occur slowly due to anthropogenic impact and the incoming seawater. Eventually, it can force a closing of some wells. It is further suggested that for some wells, the immediate threat may be the water level decline rather than water quality problems (Peter et al., 2005).

d- Simulated regional groundwater flow

The calibrated final model can be used to quantify various aspects of the conceptual model and to draw conclusions about regional groundwater flow in the aquifer system. Relative magnitudes (or volumes) of regional groundwater flow are not apparent from the map of regional groundwater flow patterns. Discharge vectors that illustrate the relative magnitude and resultant direction of horizontal regional flow within each cell are shown in Figure 14a. The lengths of these discharge vectors are scaled linearly; units are m^3/min. The greatest magnitudes of horizontal regional groundwater flow in the aquifer are associated with the Mediterranean sea boundary (northeastern part, Figure 14 a). Flow from the sea towards the groundwater system can pollute. Therefore, the model doesn't predict the future conditions with pumping but with the same discharge rate. Simulated discharge vectors indicate high magnitudes of horizontal groundwater flow in areas around the regional potentiometric highs (Figure 14 a). Discharge vectors indicate that the magnitudes of horizontal regional groundwater flow in the western, southwestern and part of the

Table 4. The water budget estimation by Modflow processing.

FLOW TERM	IN	OUT	IN-OUT
CONSTANT HEAD	9.4788672E+03	9.8457646E+03	-3.6689746E+02
WELLS	0.0000000E+00	4.5980000E+00	-4.5980000E+00
RECHARGE	3.7620456E+02	0.0000000E+00	3.7620456E+02
ET	0.0000000E+00	4.7021275E+00	-4.7021275E+00
SUM	9.8550713E+03	9.8550645E+03	6.8359375E-03

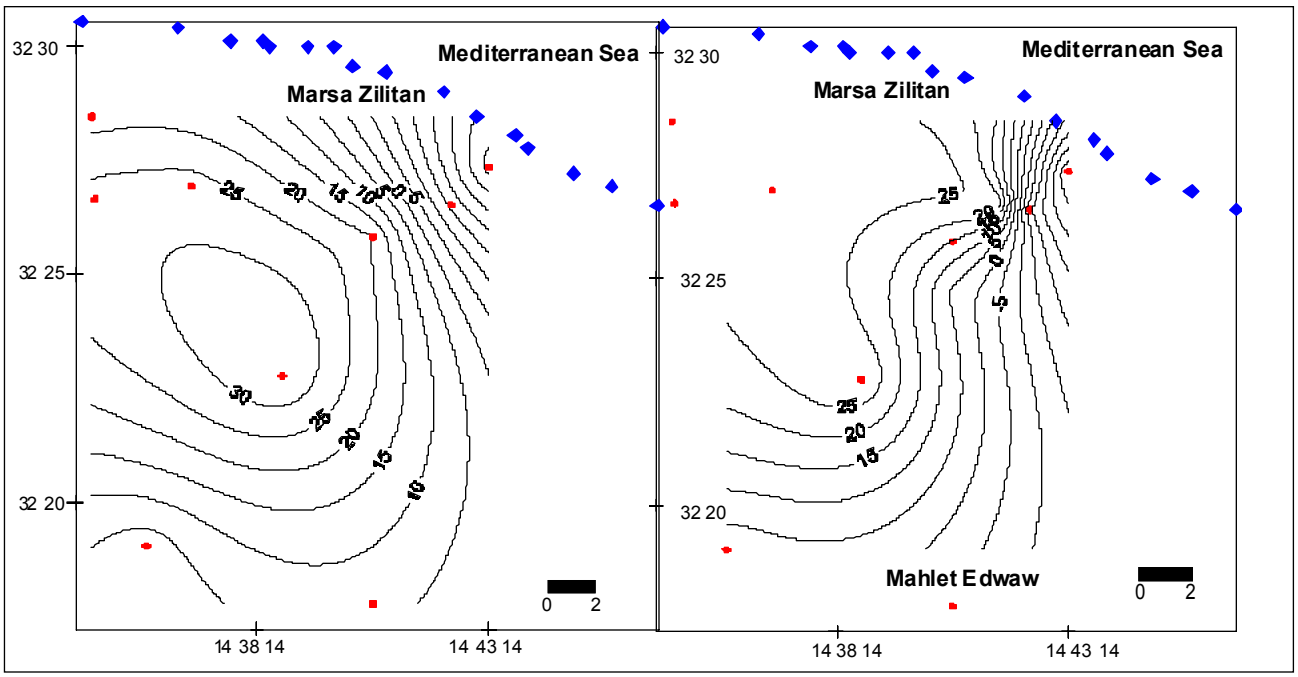

Table 15. Potentiometric level (a) and simulated level after 10 years of same current pumping rate (b).

eastern parts (Figure 14 a) are fairly small. Groundwater flow may be predominantly vertical in latter areas, because of rainfall leaking downward into the exposed limestone.

CONCLUSIONS AND RECOMMENDATIONS

Rapidly increasing urban population growth rates over the last few decades have been responsible for the production of huge quantities of wastewater, which are disposed into groundwater system without treatment. Carbonate aquifers are particularly vulnerable to nitrate contamination. The hydro geologic properties that improve in the western and eastern parts of the Zilitan area, are attributed to much more dissolution of exposed carbonate sediments. They enhance the aquifer permeability and therefore the transmissivity. TDS increases along the flow path (due north) from the surface to the saturated zone and through the aquifer system because of dissolution of minerals. Additional processes such as evaporation, evapotranspiration, or seawater intrusion, can increase the concentration of solutes. The saturation indices for calcite and dolomite are generally correlated with dissolved solid concentrations. The dedolomitization process is common in this aquifer system. The groundwater samples are suitable for irrigation purposes in good soil permeability and moderate to high drainage condition. The PMWIN model predicts the 5 m drop in potentiometric level at the southeastern part of the study area and little drop in the northeastern part (coastal part). The PMWIN model suggest no increase in pumping rates, otherwise, seawater intrusion is enhanced.

ACKNOWLEDGMENTS

This paper was reviewed by Professor Hanfy Deabass and Professor Mohamed El-Saaed in the National research institute of Astronomy and Geophysics in Helwan, Egypt

REFERENCES

Abdel-Lattif, A., Minas, H., and A. Shedid. 2004. Quantitative morphometry and flashflood probability in wadi Libda and wadi Suq Al Khamis, east al Khams city, Libya. Bull. Of Fac. of Sci., Zagazig,University, 15p.

Appelo, C. A., and A. Postma. 2005. Geochemistry, groundwater, and pollution. 2nd edn. A.A. Balkema, Amsterdam, 649p.

Back, W., B.B. Hanshaw, L.N. Plummer, P.H. Rahn, C.T. Rightmire, and M. Rubin. 1983. Process and rate of dedolomitization mass transfer, and 14C dating in a regional carbonate aquifer: Geol Soc of Amer Bull, v 94, pp. 1415-1429.

Berryhill, W.S. 1989. The impact of agriculture practices on water quality in karst region. In: Bech BF (ed) Engineering and Environmental Impacts of sinkholes and karst. Proceeding of the 3rd multidisciplinary conference, Balkema, Rotterdam.

Bierschenk, W. 1964. Determining well efficiency by multiple step drawdown test. Publication 64.International Association of Scientific Hydrology.

Burdon, D.J., and R. Gonfiantini. 1991. Lakes in the Aubari and sea of Fezzan, Libya. In the geology of Libya. Elsevier, Amsterdam, pp. 2027-2041.

Burollet, P.F. 1960. Laxique stratigraphue International, VdIV,: Africa . Part IV: Libya. Congr Geol Inte Commision De Strat rech Sci , pp. 1-62.

Burollet, P.F. 1963. Excursion to Gabal Nefusa. Guidebook of petrol Explor Soc Libya, 19p.

Busby, J.F., L.N. Plummer, R.W. Lee, and B.B. Hanshaw. 1991. Geochemical evolution of water in the Madison aquifer in parts of Montana, south Dakota, and Wyoming. USGS Professional Paper 1273-F, 89p.

Chiang, W., and W. Kinzelback. 1996. User's manual, processing mudflow, a simulation system for modeling groundwater flow and pollution. Scientific Software Group, Washington DC.

Durov, S.A. 1948. Classification of natural waters and graphic representation of their composition. Doklady Akad.Nurak, USSK, No.1.

El-Hinnawy, M., and G. Chesthitey. 1975. Geologic map of Libya, 1:250000 sheet Al Khums NI 33- 14. Explanatory booklet, Intern. Research Center, 65p.

El Shamy, I.Z., and M. Abdel Kader. 1999. Hydrogeological studies on El Maghara area. 4th Int. conf. on Geochemistry, Alex Univ., pp. 319-334.

Freeze, R.A., and J.A. Cherry. 1979. Groundwater: Englewood Cliffs, New Jersey, Prentice- Hall Inc. 213p.

Fry, A. 2005. Water facts and trends, World Business Council for sustainable Development: 16.

Goudarzi, G.H. 1970. Geology and mineral deposits of Libya, a reconnaissance: USGS Prof. pap 66D, 104pp., 78 Figure morphology: Geol. Soc. Am. Bull., v 56, pp. 275-370.

Hammuda, O.S. 1967. Jurassic and Lower Cretaceous geology of central Gabal Nefusa, northwestern Libya. M. Sc. Thesis., Colorado University, Boulder, Colorado.

Jacob, C. 1946. Drawdown test to determine the effective radius of an artesian well. Transactions of the American Society of Civil Engineers, 112, 1047-1070pp.

Katz, B.G., J.K. Bohlke, and H.D. Homsby. 2001. Timescales for nitrate contamination of spring waters, northern Florids. Chem Geol 179 (1-4): 167-186.

Liu, W.X., X.D. Li, Z.G. Shen, D.C. Wang, O.W. Wai, and Y.S. Li. 2003. Multivariate statistical study of heavy metals enrichment in sediments of the Pearl river Estuary. Environ Pollut 121: 377-388.

Magnier, A. 1963. Etud stratigraphue dansele Gebel Nefousa Etle Gable Garian (Tripolitaine, Libya). Bull. Soc. Fr., ser. 7, v 5, no. 2, pp. 89-94.

Mann, K. 1975. Geological map of Libya. Explanatory booklet, Industrial Research center, Libyan Arab Republic, 88p.

Molerio, L.F., and S. Gutierrez. 1999. Agricultural impacts on Cuban karstic aquifer. In: Drew D, Hotzl HAAA (eds) Karst hydrogeology and human activities, Balkema, Rotterdam.

Pacheco, A.J., and S.A. Cabrera. 1997. Groundwater contamination by nitrate in the Yucatan Penisnsula, Mexico. Hydrogeol J 5: 47-53.

Peter, B., H. Rudolf, Z. Stephanie, H. Flenner, and W. Kinzelback. 2005. Coupled flow and salinity ransport

modeling in semi-arid environments: The Shashe river valley, Botswana. J. Contaminant Hydrology, 13p.

Piper, A. 1944. A graphical representation in the geochemical interpretation of groundwater analysis.Am. Geophysical Union Transactions, 25:914-923.

Plummer, L.N., B.F. Jones, and A.H. Truesdell. 1976. Wateq, FA FORTRAN IV version of WATEQ, a computer program for calculating chemical equilibrium of natural waters, (revised and reprinted Jan. 1984), U.S. Geol. Survey Water resources Investigations, Report 76-13, 61p.

Ruiz, F. 2001. Trace metaks in estuarine sediments from the southeastern Spanish coast. Mar Pollut Bull 42 (6): 482-489.

Salem, O., E. Belaid, and M. Mejrbi. 2000. Hydrogeological properties of Kikla aquifers in Beni Walid-Tawighra area, northwestern Libya. 5th International conference on the Geology of the Arab World, pp.875-882.

Salem, O. 2004. Management of shared groundwater basins in Libya. African Water Journal, v 1,pp. 106-117.

Sandra, M.B., and L.L. George. 2000. Regional groundwater flow and geochemistry in the Midwestern basins and Arches aquifer system in parts of Indiana, Ohio, Michigan, Illionois. U.S. geological Survey, Professional paper, 1423-C, 100p.

Schoeller, H. 1963. Geochimie des eaux souterraines, Technip, Paris, 132p.

Shine, J.P., R.V. Ika, and T.E. Ford. 1995. Multivariate statistical examination of spatial and temporal patterns of heavy metals contamination in New Bedford Harbour marine sediments. Environ Sci.technol 29: 1781-1788.

Suleiman, A.S. 1993. Geophysics of the rifts associated with the Sirt basin (north Africa) and the Andaraco basin (north America). Doctoral dissertation, 150p.

Suleiman, A.S. 2006. Gravity investigations of the Sirt basin rift system, northern and central Libya. Intern. Conf. Geol. Arab World, Cairo University, pp169-174.

Veni, G., H. DuChene, N.C. Crawford, C. Groves, G.N. Huppert, E.N. Kastning, R. Olson, and B.J. Wheeler. 2001. Living With Karst: A Fragile Foundation. Alexandria, VA: American Geological Institute.

Wells, E.R., and S. Krothe. 1989. Seasonal fluctuation in ä15N of groundwater nitrate in a mantled karst aquifer due to macropore transport of fertilizer derived nitrate. J. Hydrol.112: 191-201.

White, W.B. 1988. Geomorphology and hydrology of karst terrains. Oxford University Press, NY.

Zhou, H.Y., X.T. Peng , and J.M. Pan. 2004. Distribution, source, and enrichment on some chemical elements in sediments of the Pearl River Estuary. China Continental Shelf Res, 24: 1857-1875.

US salinity laboratory Staff. 1954. Diagnosis and improvement of saline and alkalisoils, US Dept. Agr.Handbook. V. 6, Washington DC, pp.1-60.

Wilcox, L.V. 1948. The quality of water for irrigation use. U.S. Dept. Agric. Tech. Bull. no. 962, Washington, D.C. 40 p.

ADDRESS FOR CORRESPONDENCE
A. Abdel-Lattif
National Research Institute of Astronomy and Geophysics
(NRIAG)
Helwan, Cairo
Egypt

Email: aiman_aziz21@yahoo.com